New RADFET Dosimeter Design For Radioactive Environment Monitoring Applications

M. Meguellati, F. Djeffal, D. Arar, F. Douak and L. Khettache

Abstract— **In this paper, a radiation sensitive FET (RADFET) dosimeter design (called the Dual-Dielectric Gate All Around DDGAA RADFET dosimeter) to improve the radiation sensitivity performance and its analytical analysis have been proposed for RADFET dosimeter-based applications (monitoring, robotics, medical sciences,…). The proposed device and the Artificial Neural Networks (ANNs) have been used to study and show the impact of the proposed dosimeter on the environment monitoring and remote sensing applications. The obtained results make the DDGAA RADFET dosimeter a promising candidate for environment monitoring applications.**

Index Terms— **dosimeter, RADFET, traps, irradiation, sensitivity, Genetic Algorithm, ANNs.**

I. INTRODUCTION

The Gate All Around GAA MOSFETs have emerged as excellent devices to provide the electrostatic integrity needed to scale down transistors to minimal channel lengths, and allowing a continuous progress in digital and analog applications. In addition to a better electrostatics than the conventional bulk MOSFET, the use of these devices have advantages relative to the electronic transport, mainly due to (i) the reduced surface roughness scattering because the lower vertical electric field and (ii) the reduction of the Coulomb scattering because the film is made of undoped/low-doped silicon [1-5]. Design and modeling guidelines of GAA MOSFETs have been discussed in previous work [2-5]. Employing this design for environment monitoring applications (irradiation measurement) becomes more beneficial if the device is made in vertical cylindrical recrystallized silicon due to highly flexible process integration options. There have been several reports of MOSFETs fabricated in recrystallized silicon for high-density digital integrated circuits [5].

Radiation sensitive MOSFETs (RADFETs) have been focus of interest both from applications and fundamental research point of views. In electronic industry these devices are considered as attractive alternatives for nuclear industry, space, radiotherapy and environment monitoring applications due to their reliability, low power consumption, non-destructive read-out of dosimetric information, high dose range, and compatibility to standard CMOS technology and on-chip signal processing [6-8]. The main RADFET disadvantage is the relatively low sensitivity. In this context, the submicron multi-gate design may be considered as attractive alternative to overcome this disadvantage because of the high electrical performance and reliability provided by the multi-gate structure in comparison with single-gate one. However, as semiconductor devices are scaled into the deep submicron domain, short-channel effects (SCEs) begin to plague conventional planar CMOS-based devices. To avoid the electrical constraints and improve the sensitivity performance, a new design and enhancement of conventional (bulk) RADFET become important. In this work, a new design of RADFET called the Dual-Dielectric Gate All Around (DDGAA) RADFET dosimeter, in which the manufacturing processes and sensitivity performances will be greatly improved, is proposed for deep submicron CMOS-based dosimeter applications. The (DDGAA) RADFET dosimeter design presented in this paper is basically surrounded dual-dielectric layers (SiO2 and Si3N4) with low p-channel (Si) doping concentration. The results showed that the analytical model is in agreement with the 2-D numerical simulation over a wide range of device parameters. The proposed structure has been analyzed and validated by the good sensitivity and electrical performance obtained in deep submicron regime in comparison with the conventional (bulk) design. In addition, in this work, we present the applicability of genetic algorithm optimization (GA) approach to optimize the radiation sensitivity of the DDGAA RADFET for integrated CMOS-based dosimeters. Finally, the proposed dosimeter model was used to study and show the impact of the proposed design on the environment monitoring applications.

II. THEORY DEVELOPMENT AND MODEL DERIVATION

A. Interface potential analysis

Schematic cross-sectional view of the proposed (DDGAA) RADFET dosimeter is presented in Fig.1. The insulator consists of a thermal oxide (SiO_2) grown on a (100) n on n+ expitaxial silicon substrate (channel), and a low pressure CVD silicon nitride layer(Si_3N_4) deposited on top of the oxide. $N_{D/S}$ represents the doping level of the drain/source

region, respectively. The channel region is bounded by source and drain spacing at x= 0 and L, respectively, where L is the gate length. With a negatively applied gate bias, holes generated in the SiO_2 layer are transported and trapped at the SiO_2 /Si_3N_4 interface producing a measurable threshold-voltage shift as it is shown in Fig. 1. The investigation reported in this work for gamma radiation sources can also be applied qualitatively to other radiation sources (protons, electrons, …).
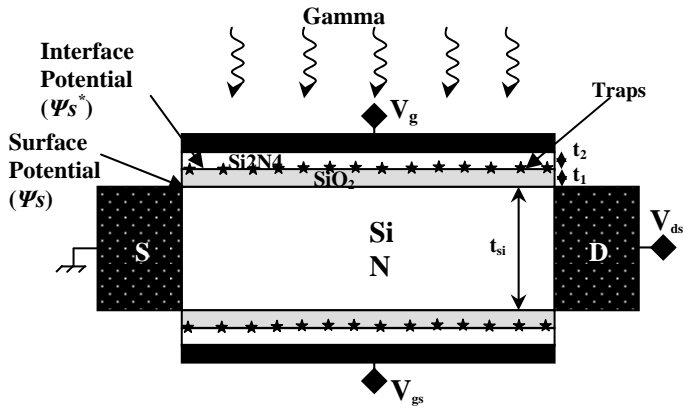
Fig 2.   Cross-sectional view of the proposed DDGAA RADFET design

For deep submicron devices, the solution of 2D Poisson's equation satisfying suitable boundary conditions is required to model the interface potential. Refer to Fig. 1, the 2D Poisson's equation for the channel region is given by

$$\frac{1}{r}\frac{\partial}{\partial r}\left(r\frac{\partial}{\partial r}\psi(r,x)\right)+\frac{\partial^2}{\partial x^2}\psi(r,x)=\frac{q\cdot N_D}{\varepsilon_{si}} \quad (1)$$

The boundary conditions for $\psi(x,r)$ are found by satisfying continuity of both the normal component of the electric displacement at the (Si/SiO_2) interfaces, and the potential at the source/drain sides.

Using the same parabolic potential profile in vertical direction [2] and applying the symmetry condition of $\partial\psi/\partial r = 0$ for $r=0$, we obtained the following expressions of 2-D channel potential as

$$\psi(r,x)=\frac{C_{ox}}{\varepsilon_{si}\cdot t_{si}}\left[V_g^* -\psi_s(x)\right]r^2+\left(1+\frac{C_{ox}t_{si}}{4\varepsilon_{si}}\right)\psi_s(x)-\frac{C_{ox}t_{si}}{4\varepsilon_{si}}V_g^* \quad (2)$$

where $\psi_s(x)$ represents the surface potential, C_{ox} represents the insulator capacitance ($C_{ox}=2\pi\varepsilon_l L/\ln(1+2t_1/t_{si})$), t_{si} is the silicon thickness, the effective oxide and silicon nitride layer is defined as $t_{oxeff}=t_1+t_2(\varepsilon_1/\varepsilon_2)$ with t_1 is the thickness of the SiO_2 ($\varepsilon_1=\varepsilon_{ox}$) layer and t_2 is the thickness of the Si_3N_4 layer (ε_2), V_{bi} is the junction voltage between the source/drain and intrinsic silicon, $V_{bi}=(kT/q)\ln(N_{D/S}/n_i)$, n_i is the intrinsic silicon density, V_{ds} represents the drain-to-source voltage and k is the Boltzmann constant. V_g^* represents the effective voltage at the gate which is introduced to simplify notations and alleviate derivations for symmetric structure as $V_g^*=V_{gs}-V_{fb}$, with V_{fb} is the flat-band voltage.

Substituting (2) in (1), we obtain the differential equation that deals only with surface potential as

$$\frac{d^2\psi_s(x)}{dx^2}-\frac{1}{\lambda^2}\psi_s(x)=D_1 \quad (3)$$

with $\lambda=\sqrt{\frac{\varepsilon_{si}\cdot t_{oxeff}\cdot t_{si}}{4\cdot\varepsilon_{ox}}}$ and $D_1=\frac{q\cdot N_D}{\varepsilon_{si}}-\frac{1}{\lambda^2}\cdot V_g^*$

where λ represents the natural length of the analyzed (DDGAA) RADFET dosimeter. This parameter gives the scaling capability (downscaling ability) of the device. D_1 is a factor which represents the impact of the applied gate voltage and channel doping on the surface potential.

The differential equation that deals only with interface potential is given by

$$\frac{d^2\psi_s^*(x)}{dx^2}-\frac{1}{\lambda^2}\psi_s^*(x)=D_2 \quad (4)$$

with $D_2=\alpha-\beta V_{gs}^*$ and $\alpha=\frac{qN_D\varepsilon_2 t_1}{\varepsilon_{si}(\varepsilon_2 t_1+\varepsilon_1 t_2)}$, $\beta=\frac{\varepsilon_2 t_1}{\lambda^2(\varepsilon_2 t_1+\varepsilon_1 t_2)}$

where ψ_s^* represents the interface potential at SiO_2 /Si_3N_4 interface which satisfies the continuity of the normal component of the electric displacement at the interface.
This resolution of this Equation allows us the calculation of the interface potential without (before) irradiation.
In the case of RADFET under irradiation new term should be introduced in order to include the radiation-induced interface-traps effect [2]. So, the parameter D_2 can be written, in this case, as, $D_2=\alpha-\beta V_{gs}^*-qN_f/\varepsilon_2 t_2$, with N_f represents the irradiation induced localized interface charge density per square area. The second term in this expression represents the impact of the irradiation induced localized interface charge density on the interface potential.
The surface and interface potentials can be, respectively, expressed as

$$\psi_S(x)=-\lambda^2 D_2+\frac{\phi_D \sinh\left(\frac{x}{\lambda}\right)-\phi_S \sinh\left(\frac{x-L}{\lambda}\right)}{\sinh\left(\frac{L}{\lambda}\right)} \quad (5)$$

With $\phi_D=V_{ds}+\lambda^2 D_2$ and $\phi_S=V_{bi}+\lambda^2 D_2$

$$\psi_S^*(x)=\frac{\varepsilon_1 t_2}{\varepsilon_2 t_1+\varepsilon_1 t_2}V_{gs}^*+\frac{\varepsilon_2 t_1 x}{\varepsilon_2 t_1+\varepsilon_1 t_2}\psi_S(x) \quad (6)$$

B. Threshold voltage shift model

Schematic cross-sectional view of the proposed (DDGAA) RADFET The basic concept of RADFET dosimeter is to convert the threshold voltage shift, ΔV_{th}, induced by radiation, into absorbed radiation dose, where $\Delta V_{th}=V_{th}-V_{th0}$ with V_{th} and V_{th0} represent the threshold voltage after and before irradiation, respectively.
Based on the surface potential model given by Eq.(5), the threshold voltage can be derived using the condition of the minimum channel potential $\psi_{smin}|_{V_{gs}=V_{th}}=2.\phi_B$, with $\psi_{smin}=\psi_s(x_{min})$, V_{th} is the threshold voltage value, and ϕ_B represents the bulk potential of silicon body given as $\phi_B=(K_B T/q).\ln(N_D/n_i)$. The location of the minimum

surface potential can be obtained analytically by solving $\dfrac{d\psi_s(x)}{dx} = 0$ [2].

The solution of the equation $\psi_{s\min}\big|_{V_{gs}=V_{th}} = 2.\phi_B$ at low drain-source voltage for long channel lengths ($L \gg \lambda$) can be given as

$$V_{th} = \frac{\left(2A\phi_B + \lambda^2\alpha + \dfrac{qN_f}{\varepsilon_2 t_2}\right)\sinh\left(\dfrac{L}{\lambda}\right) + \left(V_{bi} - V_{ds}\right)\sinh\left(\dfrac{L}{2\lambda}\right)}{\left(\beta\lambda^2 - \dfrac{B}{A}\right)\sinh\left(\dfrac{L}{\lambda}\right) - 2\sinh\left(\dfrac{L}{2\lambda}\right)} \quad (7a)$$

with: $A = \dfrac{\varepsilon_1 t_2 - \varepsilon_2 t_1}{\varepsilon_2 t_2}$, $B = \dfrac{\varepsilon_2 t_1}{\varepsilon_1 t_2}$

$$V_{th0} = V_{th}\big|_{N_f=0} = \frac{\left(2A\phi_B + \lambda^2\alpha\right)\sinh\left(\dfrac{L}{\lambda}\right) + \left(V_{bi} - V_{ds}\right)\sinh\left(\dfrac{L}{2\lambda}\right)}{\left(\beta\lambda^2 - \dfrac{B}{A}\right)\sinh\left(\dfrac{L}{\lambda}\right) - 2\sinh\left(\dfrac{L}{2\lambda}\right)}$$

(7b)

From (7a) and (7b), the threshold voltage shift can be given as

$$\Delta V_{th} = \frac{\dfrac{qN_f}{\varepsilon_2 t_2}\sinh\left(\dfrac{L}{\lambda}\right)}{\left(\beta\lambda^2 - \dfrac{B}{A}\right)\sinh\left(\dfrac{L}{\lambda}\right) - 2\sinh\left(\dfrac{L}{2\lambda}\right)} \quad (7c)$$

III. RESULTS AND DISCUSSION
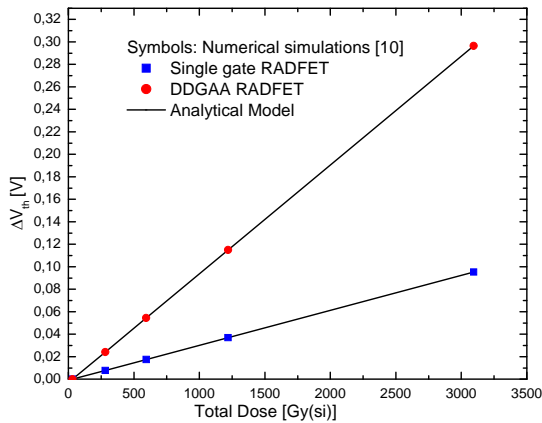
Fig 2. Variation of threshold voltage shift in function of the absorbed radiation dose for the conventional and DDGAA RADFET designs.

The RADFET radiation sensitivity S, given by [8,9]:

$$S = \frac{\Delta V_{th}}{D} \quad (9)$$

where D represents the absorbed radiation dose.

In Figure 2, the variation of DDGAA RADFET sensitivity versus the absorbed radiation dose, D, has been compared with conventional (bulk) RADFET. For both designs, the output response of the RADFETs is linear with absorbed radiation dose. It is clearly shown that DDGAA RADFET has higher sensitivity, $S = 95.45\,\mu V/Gy$, in comparison with conventional RADFET design, $S = 30.68\,\mu V/Gy$. This

means that DDGAA RADFET has better electrical and scaling performances in comparison with the conventional design. So, our design provides a high sensitivity, better electrical and technological performances in comparison with the conventional structure. These results make the proposed design as a promising candidate for CMOS-based dosimeters.

A. GA-based sensitivity optimization

GA optimization has been defined as finding a vector of decision variables satisfying constraints to give acceptable values to objective function. It has recently been introduced to study the complex and nonlinear systems and has found useful applications in engineering fields. Due to the simple mechanism and high performance provided by GA for global optimization, GA can be applied to find the best design of DDGAA RADFET in order to improve the radiation sensitivity by satisfying of the following objective function:

- Maximization of the RADFET radiation sensitivity $S(X)$

Where X represents the input normalized variables vector which is given as $X = (t_{si}, t_1, t_2, L)$.

For the purpose of GA-based optimization of the radiation sensitivity of DDGAA RADFET, routines and programs for GA computation were developed using MATLAB 7.2 and all simulations are carried out on a Pentium IV, 3GHz, 1GB RAM computer. For the implementation of the GA, tournament selection is employed which selects each parent by choosing individuals at random, and then choosing the best individual out of that set to be a parent. Scattered crossover creates a random binary vector. It then selects the genes where the vector is unity from the first parent, and the genes where the vector is zero from the second parent, and combines the genes to form the child. An optimization process was performed for 20 population size and maximum number of generations equal to 200, for which stabilization of the fitness function was obtained.

The steady decrease in objective function in each generation until it reaches a best possible value can be attributed to the selection procedure used namely Roulette wheel selection.

TABLE II
DDGAA RADFET DESIGN PARAMETERS

Symbol	Optimized design	Design without optimization	Conventional design
$L(nm)$	100	100	100
$t_{si}(nm)$	50	20	20
$t_1(nm)$	5	5	5
$t_2(nm)$	15	5	-
$S(\mu V/Gy)$	162.22	95.45	30.68

The radiation sensitivity values of the DDGAA RADFET with and without optimization are shown in Table. 1. It is clearly shows that The radiation sensitivity, for optimized design (162.22 $\mu V/Gy$) is better than the both conventional RADFET ($S = 30.68\,\mu V/Gy$) and DDGAA RADFET without optimization ($S = 95.45\,\mu V/Gy$).

B. Radioactive environment sensing

In order to show the impact of the proposed design on the radioactive environment monitoring, we propose the study of a contemned radioactive environment. This latter is considered a big challenge in the field of the environment monitoring. In this work, using simulated database (built from numerical data) of total dose radioactivity distribution in 2-D space and the Multi-Layer-Perception (MLP) tool, we will study a contemned environment by gamma radiation.

Artificial neural network (ANN) based methods have been widely used for modeling various complex and nonlinear processes (classification, speech recognition, and signal processing). The model based on artificial neural network [10-12] assumes that input and output patterns of a given problem are related by a set of neurons organized in hidden layers. The layers in these networks are interconnected by communication links that are associated with weights that dictate the effect on the information passing through them. These weights are determined by the learning algorithm.

The output of node *j* in the hidden layer is given by

$$h_j = g\left(\sum_{i=14}^{n} w_{ij} . x_i + b_j \right)$$

And the output of the network by

$$y = \sum_{i=14}^{k} wo_i . h_i$$

Where w_{ij} are the weights connecting the inputs to node *j* in the hidden layer, b_j is the bias to the node, and wo_i are the weights from the hidden to the output layer.

The activation function relates the output of a neuron to its input based on the neuron's input activity level. Some of the commonly used functions include: the threshold, piecewise linear, sigmoid, tangent hyperbolic, and the Gaussian function [11]. The learning process of the MLP network involves using the input–output data to determine the weights and biases. One of the most techniques used to obtain these parameters is the back-propagation algorithm [11– 13]. In this method, the weights and biases are adjusted iteratively to achieve a minimum mean square error between the network output and the target value.

The energy recorded by the sensor has to be transmitted, often in electronic form, to a receiving and processing station, where the data are processed into an image. Radiation that is not absorbed or scattered in the atmosphere can reach and interact with the Earth's surface. There are three forms of interaction that can take place when energy strikes, or is incident upon the surface [14].

In remote sensing, we are most interested in measuring the radiation reflected from targets. This reflection disgusting the image caption by the sensors (which are located at reception stations), we propose that interacting energy (noise) is a Gaussian noise.

In this work, the artificial neural network is used to denoising the image distorted by the transmission noise (Fig. 4). In this context, the database for MLP optimization consists of 49600 samples split into three categories: training, validation and test sets. The training and validation are used tune MLP configuration and the test is used to test the MLP configuration to denoise the different regions of the contemned environment. Test and training steps were run for a given MLP structure to obtain the optimal MLP configuration. The database is collected from several RADFETs, which have been located in different regions in the contemned environment. In order to validate the denoising proprieties of the optimized MLP, test set is compared to the MLP response.

Fig.5 presents the space distribution of the gamma radiation in the investigated contemned environment after the denoising process. It is shown that the different regions are clearly represented. This last observation shows the applicability and the efficiency provided by the MLP-based approach to study the radioactive environment.

Fig. 6 shows that a good agreement between MLP and real results is found. Hence, the optimized structure can be used for the radioactive environment monitoring applications.

Fig 4. The distorted image due to the transmission noise.

Fig 5. The denoised image using MLP.
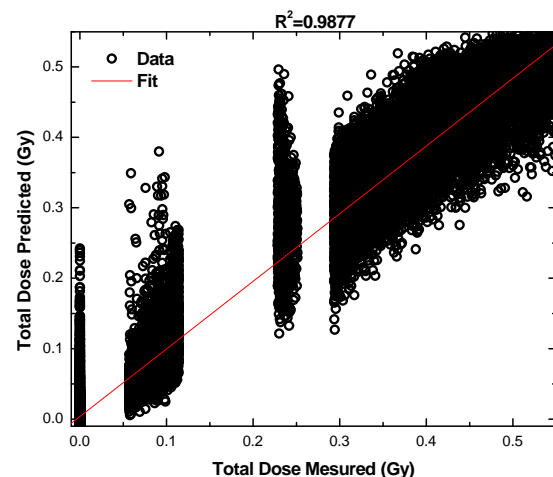
Fig 6. Validation of the neural network result for test set.

IV. CONCLUSION

In this paper, we compared new sensor design, DDGAA RADFET, with conventional planar RADFET through 2-D analytical investigation. A two-dimensional analytical analysis comprising radiation-induced interface-traps effect, 2D surface and interface potentials, threshold voltage shift and sensitivity model for DDGAA RADFET has been developed. The threshold voltage shift behavior of the proposed design was more effectively improved than those of the conventional planar RADFET. Also, we confirmed that DDGAA RADFET had advantages in CMOS scaling in comparison with planar RADFET. Application of the GA-based design approach to DDGAA RADFET has also been discussed. It can be concluded that proposed GA-based approach is efficient and gives the promising results. In order to show the impact of the proposed design on the radioactive environment monitoring, we developed a MLP-based approach to study a contemned radioactive environment. The proposed approach can be used for remote sensing applications, where the information about the contemned radioactive environment should be transmitted in electronic form to a receiving and processing station.

REFERENCES

[1] The international technology roadmap for semiconductors (ITRS); 2007. <http:// public.itrs.net>.

[2] Z. Ghoggali, F. Djeffal, N. Lakhdar, Analytical analysis of nanoscale Double- Gate MOSFETs including the hot-carrier degradation effects, Int. J. Electronics, pp. 119-127, 97(2), 2010.

[3] D. Jiménez, B. Iñiguez, J. Suñé, L.F. Marsal, J. Pallarès, J. Roig and D. Flores, Continuous Analytic I-V Model for Surrounding-Gate MOSFETs, IEEE Electron Devices Letters, Vol.25, pp. 571-573, 2004.

[4] H. Kaur, S. Kabra, S. Haldar and R.S. Gupta, An analytical drain current model for graded channel cylindrical/surrounding gate MOSFET, Microelectronics Journal, vol. 38, pp. 352-359, 2007.

[5] MA. Abdi , F. Djeffal, D.Arar, ML. Hafiane, Numerical analysis of Double Gate and Gate All Around MOSFETs with bulk trap states. J Mater Sci: Mater Electron, vol. 19, pp. S248-S253, 2008.

[6] F. Djeffal, T. Bendib, M. Meguellati, D. Arar and M.A Abdi, New Dual-Dielectric Gate All Around (DDGAA) RADFET Dosimeter Design to Improve the Radiation Sensitivity, Proceedings of the World Congress on Engineering 2012 Vol II WCE 2012, July 4 - 6, 2012, London, U.K., pp. 917-921.

[7] A. Kelleher, W. Lane, L. Adams, A design solution to increasing the sensitivity of pMOS dosimeters: The stacked RADFET approach, IEEE Trans. Nuclear Science, vol. 42, pp.48–51, 1995.

[8] A. Jaksic, G. Ristic, M. Pejovic, A. Mohammadzadeh, C. Sudre, W. Lane, Gamma-ray irradiation and post-irradiation responses of high dose range RADFETs, IEEE Trans. Nuclear. Science, vol. 49, pp. 1356–1363, 2002.

[9] J.R. Schwank, S.B. Roeske, D.E. Beutler, D. J. Moreno, M.R. Shaneyfelt, IEEE Trans. Nuclear Science, vol. 43, pp. 2671–2678, 1996.

[10] Atlas User's manual, SILVACO TCAD, 200

[11] Guessasma S, Ghislain M, Christain C. Modeling of the APS plasma spray process using artificial neural networks: basis requirements and an example. Comput Mater Sci 2004;29:315.

[12] F. Djeffal, M. Chahdi, A. Benhaya, M.L. Hafiane. An approach based on neural computation to simulate the nanoscale CMOS circuits: Application to the simulation of CMOS inverter. Solid-State Electronics 51 (2007) 48–56.

[13] Taylor JG. Neural networks and their applications. West Sussex (UK): John Wiley & Sons Ltd.; 1996.

[14] A Canada Centre for Remote Sensing, Remote Sensing Tutorial, availble on line for free http://www.uprm.edu/biology/profs/chinea/gis/g06/NRC1_1_1_5.pdf.